CHEMISTRY OF MATERIALS

pubs.acs.org/cm

Article

Raman Spectroscopy Characterization of 2D Carbide and Carbonitride MXenes

Kateryna Shevchuk,[#] Asia Sarycheva,[#] Christopher E. Shuck, and Yury Gogotsi*

Cite This: *Chem. Mater.* 2023, 35, 8239−8247

Read Online

ACCESS | Metrics & More | Article Recommendations | Supporting Information

ABSTRACT: The first step to wider adoption of two-dimensional (2D) materials is understanding their fundamental properties by employing characterization methods, among which Raman spectroscopy plays a unique role, being a fast and nondestructive tool. The number, frequencies, and intensities of the modes (or bands) in the Raman spectrum have been used to identify the 2D materials' crystal lattice, bonding, and even number of layers. MXenes, 2D transition metal carbides, nitrides, and carbonitrides, span diverse chemistries and structures, but only a few Raman spectra have been reported. This work is the first systematic experimental Raman spectroscopy study of the MXene family. We explore the vibrational spectra and provide peak assignments for ten MXenes with varying structures (from 2 to 4 atomic layers of transition metal) and compositions—Ti_2CT_x, Nb_2CT_x, Mo_2CT_x, V_2CT_x, $Ti_3C_2T_x$, $Mo_2TiC_2T_x$, Ti_3CNT_x, $Nb_4C_3T_x$, $V_4C_3T_x$, and $Mo_2Ti_2C_3T_x$ (terminated with −F, −OH, and =O) based on the experimental results and previously reported computational studies. We discuss the effects of MXene layer thickness, surface terminations, and MXene's metallic properties on Raman scattering. Additionally, we employ polarized Raman spectroscopy to identify out-of-plane vibrations and explain the higher frequency region of the spectra. Finally, we demonstrate how electrochemical reactions affect molecular Raman scattering through the change in surface terminations. By creating the Raman spectra library of the most frequently used MXenes, we open the door for the use of Raman spectroscopy for fingerprinting and *in situ* studies of various MXenes.

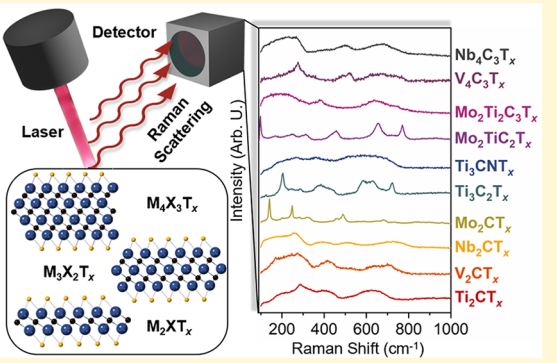

INTRODUCTION

In recent years, 2D materials have paved the way for crucial scientific and technological advances, making flexible and wearable electronics possible, advancing fundamental physics, and evolving nanomedicine. The performance of a device cannot be optimized without establishing the structure−property−performance relationship. While the link between property and performance relies on engineering design, understanding the structure−property connection requires adequate characterization. Within the field of 2D materials, Raman spectroscopy has become one of the most impactful and widely used tools. For graphene,[1] a Raman spectrum consisting of just 3 bands provides information about material quality,[2] thermal conductivity,[3] number of layers, crystallographic orientation,[4] and localized strain. In the case of transition metal dichalcogenides (TMDs), in addition to fingerprinting specific compositions and the properties described above, it is possible to couple the excitation wavelength with the band gap,[5] resulting in resonant Raman scattering. This provides information about the electronic properties of TMDs. It is evident that the structural properties of newly discovered classes of 2D materials will be probed by Raman spectroscopy.

Among novel 2D materials, MXenes have gained significant interest for use in a variety of applications, from electrochemical energy storage to biomedicine.[6] MXenes have the general formula $M_{n+1}X_nT_x$, where M is an early transition metal, X is C and/or N, n = 1−4, and T_x represents the surface termination (O, OH, halogens, and/or chalcogens). These 2D transition metal carbides, nitrides, and carbonitrides combine hydrophilic properties, redox-active surfaces, and the conductivity reaching above 20,000 S cm^{-1}.[7] The hydrophilic nature is due to the surface terminations, =O, −OH, and −F, that originate from the wet-chemical top-down synthesis, selective etching of MAX phase precursors, allowing processability from aqueous dispersions. The MXene family has been rapidly expanding, with over 50 compositions synthesized to date, and hundreds of structures predicted with varying transition metals, surface terminations, and carbon/nitrogen contents.[8]

With the MXene family growing at such a rapid pace, it is essential to establish consensus on characterization techniques.

Received: July 13, 2023
Revised: September 15, 2023
Published: September 29, 2023

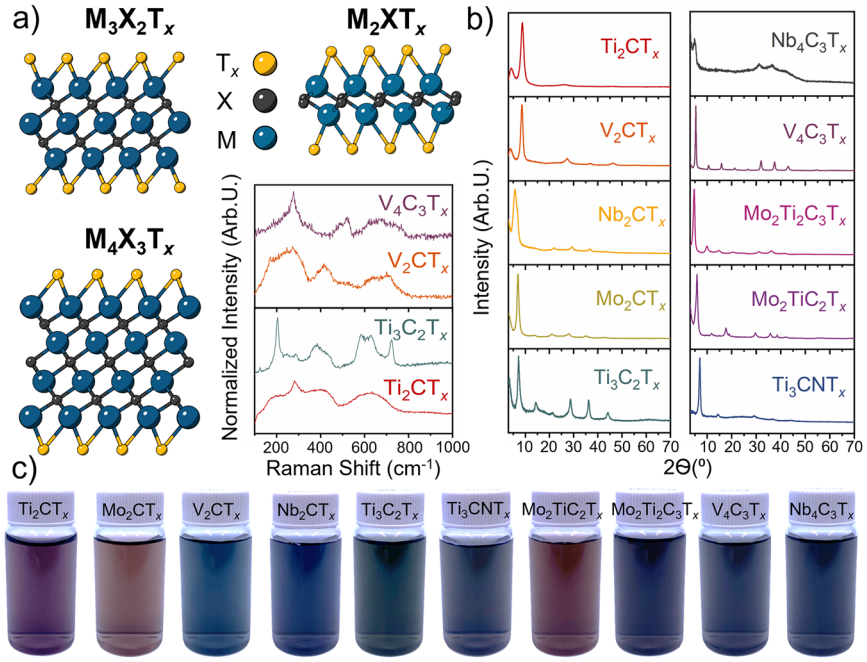

Figure 1. Overview of structures and properties of MXenes. (a) Schematics of M_2XT_x, $M_3X_2T_x$, and $M_4X_3T_x$ structures, where M is the transition metal, X is carbon and/or nitrogen, and T_x is −F, =O, and −OH groups. Examples of Raman spectra show that one can differentiate between MXenes with similar chemistries but different layer thicknesses (Ti_2CT_x vs $Ti_3C_2T_x$, V_2CT_x vs $V_4C_3T_x$). (b) XRD patterns of analyzed MXene films: the appearance of (002) peaks indicated successful synthesis and in-plane alignment of MXene flakes. (c) Colors of ∼0.1 mg/mL MXene solutions.

Multiple research groups have published extensive reviews on various characterization methods of MXenes, including Raman spectroscopy.[9,10] Our previous work focused on Raman spectroscopy analysis of the most common MXene, $Ti_3C_2T_x$, which was synthesized by various methods and processed into different morphologies.[11] More recently, we explored tip-enhanced Raman spectroscopy to analyze single- and few-layer flakes of $Ti_3C_2T_x$.[12] Computational studies on phonon dispersion and predictions of Raman spectra resulted in peak assignments for a subset of MXenes, with $Ti_3C_2T_2$ being the first explored material.[13] Berger et al. recently used machine-learning force-field molecular dynamics to predict Raman spectra of $Ti_3C_2T_x$ with heterogeneous surface terminations.[14] V_2CT_x has been analyzed using first-principles modeling, and the vibrational modes have been correlated with the experimental results.[15] Raman peaks of pristine and terminated MXenes with M_2XT_x structures (where M is Sc, Ti, Zr, Mo, and Hf, X is C, T_x is O and F) have been predicted by Yorulmaz et al.[16] Additionally, Ti_2CT_x Raman spectra have been explored in relation to bond covalency[17] and monolayer−bilayer structures.[18] The effect of Mo-substitution on optical modes has been explored for $Mo_2TiC_2O_2$.[19] The predicted Raman vibrations of Nb_2CT_x and $Nb_4C_3T_x$ have also been reported.[20] Aside from computational predictions, many works report Raman spectra as a part of the material characterization; however, in those reports Raman analysis is not a focus of the study. There has been no systematic study comparing multiple members of the MXene family experimentally and providing guidance regarding the identification of various MXenes.

In this work, we solely focus on the collection and interpretation of Raman spectra of ten MXenes: Ti_2CT_x, Nb_2CT_x, Mo_2CT_x, V_2CT_x, $Ti_3C_2T_x$, $Mo_2TiC_2T_x$, Ti_3CNT_x, $Nb_4C_3T_x$, $V_4C_3T_x$, and $Mo_2Ti_2C_3T_x$. We used the best practices and previously reported protocols to make MXenes and confirmed synthesis success and phase purity by performing X-ray diffraction (XRD) analysis. We aim to provide an experimental guide for researchers by recording characteristic vibrational spectra of free-standing films and assigning Raman-active vibrations for MXenes with different numbers of atomic layers (n = 1 to 3: M_2XT_x, $M_3X_2T_x$, and $M_4X_3T_x$ structures). We also included a carbonitride MXene (Ti_3CNT_x) and an out-of-plane double-metal MXene ($Mo_2Ti_2C_3T_x$). Among dozens of MXenes synthesized to date, the factors for choosing samples to analyze were the community interest and a wide variety of metals with not only different masses but also different electronic shells. The dependence of Raman spectra on those factors for the M_2XT_x structures is also shown. Additionally, we confirmed the nature of the out-of-plane peaks of Ti_2CT_x using polarized Raman spectroscopy and demonstrated the usefulness of Raman spectroscopy for *in situ* monitoring of electrochemical redox processes in $Ti_3C_2T_x$ MXene.

RESULTS AND DISCUSSION

To date, MXenes have been synthesized with a variety of methods, whether different wet chemical etching recipes, the more recently developed molten salt method,[21] or chemical vapor deposition[22] techniques. The most common MXene preparation procedures use acidic solutions (such as hydrofluoric acid) to selectively etch A elements (Al, Si, Ga) from the MAX phase precursors. After the etching steps, MXenes are washed with enough water to bring the pH close to neutral, resulting in a multilayer morphology. The next step includes the intercalation of Li^+, tetramethylammonium (TMA^+), or tetrabutylammonium (TBA^+) ions, with subsequent delamination into single-flake colloidal solutions. While every step of synthesis for $Ti_3C_2T_x$ has been well-defined by Alhabeb et al.,[23] the best synthesis approaches of many other MXenes are a

https://doi.org/10.1021/acs.chemmater.3c01742
Chem. Mater. 2023, 35, 8239−8247

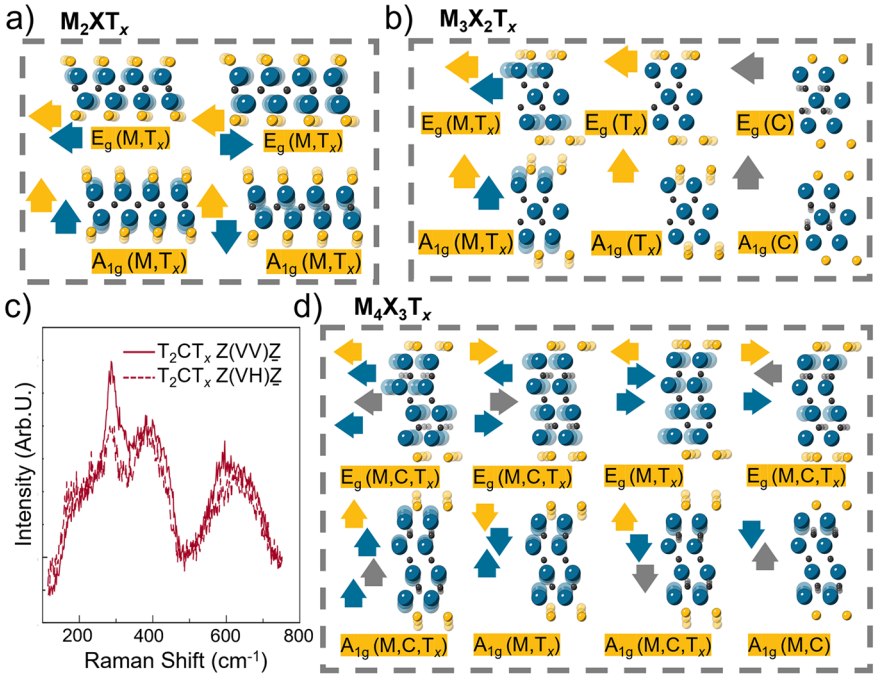

Figure 2. Raman active vibrations of MXenes and polarized Raman. (a, b, d) M_2XT_x structures exhibit four Raman-active vibrations, while $M_3X_2T_x$ structures exhibit six and $M_4X_3T_x$ structures exhibit eight Raman-active vibrations. Adapted with permission from ref 20. Copyright 2018 American Chemical Society. (c) Spectrum of Ti_2CT_x collected at different Porto notations: Z(VV)Z and Z(VH)Z were obtained using polarized Raman spectroscopy. The diminishing of the low-frequency peak indicated its A_{1g} symmetry.

work in progress.[24] All conditions for synthesizing the materials analyzed are shown in Supporting Information (Table S1) and represent the best practices from the reported work and recent unpublished developments. It can be observed that MXene synthesis parameters vary depending on the M-element, X-element, and *n* value in the MXene formula. For example, M_2XT_x MXenes are generally etched during shorter times compared to thicker $M_4X_3T_x$ MXenes.

Figure 1a shows a schematic of all of the analyzed structures: M_2XT_x, $M_3X_2T_x$, and $M_4X_3T_x$. While the surface terminations are shown to be homogeneous in the schematic, in reality, they are heterogeneously distributed =O, −OH, and −F groups. Structural differences significantly affect the Raman spectra, as can be observed in Figure 1a. While MXenes remain chemically similar, the new peak formation and broadening upon the addition of layers make Raman spectroscopy a valuable tool for distinguishing between different MXene structures.

Compared with Raman spectroscopy, XRD shows similar patterns for MXenes with different structures (Figure 1b). Broadly, all M_2XT_x MXenes will have similar XRD patterns due to the similarity of their *c*-lattice parameters. Due to the thicker structure, $M_3X_2T_x$ MXenes will have a larger *c*-lattice parameter than M_2XT_x, likewise $M_4X_3T_x$ against $M_3X_2T_x$.[9] The differences in atomic scattering factors play a role in the differing peak intensities, but for MXenes, this difference is not extreme. What these XRD patterns do indicate is that the MAX phase was etched, and the delamination of the MXenes was successful; only (00*l*) peaks are present, indicating that the MXene sheets are all aligned.[9] Thus, XRD is a good method to determine if synthesis was successful or if any impurity phases remain, but extracting significantly more information is challenging and fraught with confounding variables that complicate analysis. As previously reported,[25] MXene colloidal solutions vary in color depending on their M-site transition metal and X-element. Figure 1c shows the range of colors for ten analyzed MXenes diluted to ∼0.1 mg/mL; while M_2XT_x and $M_3X_2T_x$ structures show contrasting color palettes, $M_4X_3T_x$ MXenes possess dark grayish tones. The colors result from differences in visible light absorption spectra of MXenes.[25]

MXenes belong to the point group D_{3d}, which vibrations could be described in Mulliken symbols as $2(N-2)E_g + (N-2)A_{1g} + 2(N-2)E_u + (N-2)A_{2u}$.[13] Notably, E_g and E_u are doubly degenerate modes; therefore they appear as one in irreducible representation.[17] Only E_g and A_{1g} are Raman-active vibrations, where E_g corresponds to in-plane vibrations, and A_{1g} corresponds to out-of-plane vibrations. The thinnest M_2XT_x members of the MXene family, which have only one M-element and one X-element (e.g., Mo_2CT_x, Ti_2CT_x, Nb_2CT_x, and V_2CT_x) with no surface groups, would have three atoms per unit cell and two active Raman modes based on irreducible representations: $\Gamma_{optical} = E_g + A_{1g}$ (Figure 2b). When the number of atomic layers increases (in the case of $Ti_3C_2T_x$, $Mo_2TiC_2T_x$), the number of atoms per unit cell reaches five. This corresponds to four active Raman modes: E_g, an in-plane vibration of M atoms, and A_{1g}, an out-of-plane vibration of M atoms; two others correspond to in-plane and out-of-plane vibrations of X atoms[13] (Figure 2a). According to our knowledge, the only work exploring computational Raman predictions of $M_4X_3T_x$ structures is the study by Hu et al.[20] (Figure 2d). Without surface terminations, the structure has six active Raman modes: three out-of-plane and three in-plane vibrations. According to group theory, the middle layer of atoms (C layer in Ti_2CT_x, middle Ti layer in $Ti_3C_2T_x$, middle carbon layer in $Nb_4C_3T_x$) stays silent and does not contribute to the Raman spectrum under normal circumstances.[20] In general, E_g vibrations of a set of atoms exhibit a lower

https://doi.org/10.1021/acs.chemmater.3c01742
Chem. Mater. 2023, 35, 8239−8247

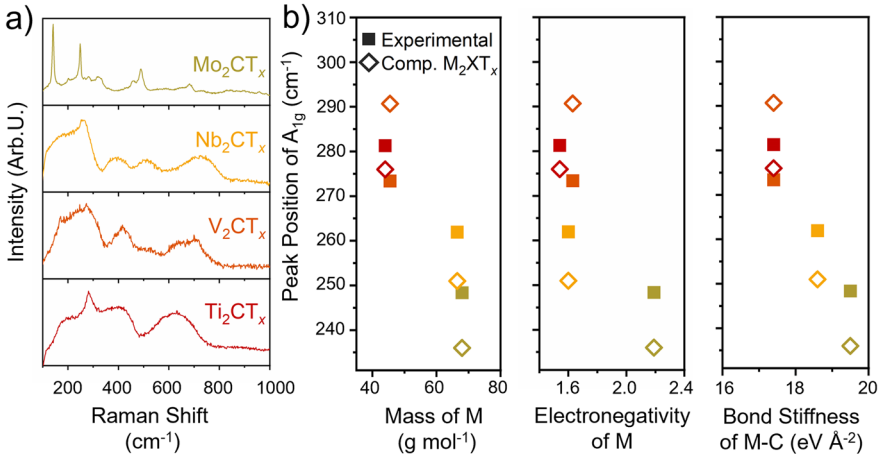

Figure 3. M_2XT_x family of MXenes. (a) Spectra of Mo_2CT_x, Nb_2CT_x, V_2CT_x, and Ti_2CT_x collected with a 514 nm laser. (b) The changes of the peak position for out-of-plane vibration with the increase in mass, change in electronegativity of an M-element and M-C bond stiffness: theoretical data (Ti_2CO_2 and Mo_2CO_2,[16] V_2CFO,[15] and Nb_2CO_2[20]) and experimental data for the symmetric A_{1g} (M, T_x) vibration.

frequency than the A_{1g} vibrations since stretching modes are stiffer than bending modes. The vibrations containing all MXene atoms but the middle layer are usually the most intense and are located at a lower frequency. The vibrations of the carbon layer (in $M_3X_2T_x$ and $M_4X_3T_x$ MXenes) appear at a higher frequency region, 500−800 cm^{-1}. When the heterogeneous surface groups (=O, −F, −OH) are added, the number of atoms in the unit cell increases; therefore, the number of vibrations should increase accordingly. The spectral predictions become complex and require significant computational work to account for the peak broadening caused by the superposition of vibrations of different surface groups. Other techniques can be explored to confirm the peak assignment.

To distinguish in-plane and out-of-plane vibrations, one can employ polarized Raman spectroscopy, also known as Raman crystallography. It utilizes the relationship between the polarization of the incident light and the scattered light, which depends on the symmetry of vibration as well as the orientation of the crystal.[26] In the case of MXenes, the E_g vibrations depolarize scattering whereas A_{1g} vibrations inherit the polarization of the incident laser. In other words, since the initial laser polarization is set vertically, the scattering of the A_{1g} vibration exhibits only vertical polarization, while scattering from E_g vibrations exhibits both vertical and horizontal components (Figure S1). Therefore, if we filter out all vertical polarization in Raman scattering, the intensity of the A_{1g} vibrations will diminish, making it possible to identify A_{1g} vibrations. Figure 2c shows that Ti_2CT_x peaks at around 300 and 600 cm^{-1} are A_{1g} out-of-plane vibrations, and the rest of the M_2XT_x structures analyzed follow the same pattern.

Figure 3a shows Raman spectra collected from free-standing films of Ti_2CT_x, Mo_2CT_x, Nb_2CT_x, and V_2CT_x. It is important to note that although the presented spectra were collected from one sample, the Raman spectra of all MXenes were monitored to ensure that the spectra have batch-to-batch reproducibility. The spectra of V_2CT_x, Ti_2CT_x, and Nb_2CT_x contain four broad peaks, which, according to DFT calculations,[15,20] represent two sets of out-of-plane vibrations and two sets of in-plane vibrations. For the V-, Ti-, and Nb-MXenes the in-plane vibration of transition metal atoms produces a broad peak at 160−180 cm^{-1} overlapping with the A_{1g} peak, which makes the exact position assignment challenging. The A_{1g} vibrations located in the low-frequency region at around 280 cm^{-1} are labeled symmetric and represent the out-of-plane vibration of transition metal atoms. Previous reports have discussed some discrepancies in the assignment of E_g and A_{1g} vibrations for other M_2X structures in the 100−300 cm^{-1} region;[27] however, according to the theoretical calculations and polarized Raman spectroscopy results, the lower-frequency peak in that region corresponds to in-plane vibration, followed by the out-of-plane vibration peak. Additionally, it has been shown computationally that the surface terminations weaken the motion of M and X atoms,[16,17] redshifting those low-frequency region peaks. The broad peaks at 400−500 cm^{-1} are indicative of terminated MXenes and represent the vibration of all atoms in the monolayers. A_{1g} vibrations in higher frequency regions (600−700 cm^{-1}) are labeled asymmetric and only appear in terminated M_2XT_x structures.[16] While Mo_2CT_x follows that general pattern (four peaks at similar ranges), much sharper peaks are observed, which could be due to the resonance effect.

The resonance Raman effect occurs when the laser wavelength matches or is somewhat shorter than the optical transition wavelength of the material. This effect has been extensively studied for nanomaterials; for example, resonant conditions in MoS_2 were achieved with more than one laser.[28] Ultraviolet−visible (UV−vis) spectroscopy has previously shown Mo_2CT_x transition wavelength at 450 nm,[25] and Velusamy et al. reported the transversal plasmon resonance at 506 nm for Mo_2CT_x.[29] In this study, the 514 nm laser wavelength can lead to the resonance effect in Mo_2CT_x, increasing the intensity of the fundamental peaks and leading to the appearance of smaller peaks, which could be combinations and overtones. Mo_2CT_x spectra using three other lasers can be seen in Figure S2: while the peaks remain sharp, their number decreases. Advanced computational studies are needed to further understand this phenomenon in Mo_2CT_x.

As previously mentioned, the out-of-plane nature of the low-frequency A_{1g} (M, T_x) symmetric vibration was confirmed with the polarization experiment, and the resulting peak depends on the transition metal of the MXene. The changes in the position of the vibration with the increase of the mass of a transition metal (Ti < V < Nb < Mo), the electronegativity of a transition

https://doi.org/10.1021/acs.chemmater.3c01742
Chem. Mater. 2023, 35, 8239−8247

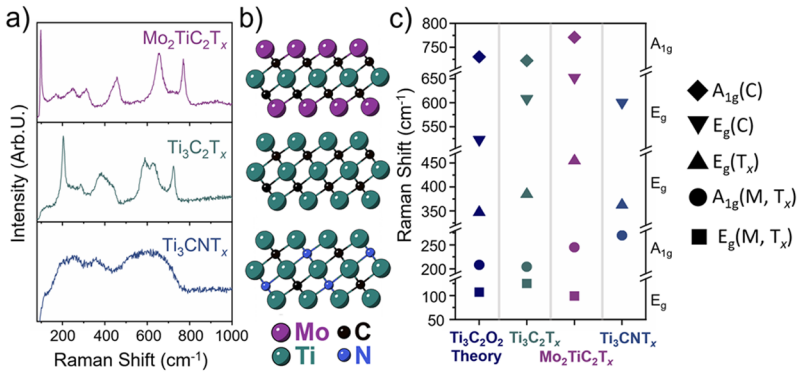

Figure 4. $M_3X_2T_x$ family of MXenes. (a) Raman spectra of $Mo_2TiC_2T_x$, $Ti_3C_2T_x$, and Ti_3CNT_x collected with a 514 nm laser. (b) Structure schematic of three analyzed MXenes: $Ti_3C_2T_x$ structure with the outer layers of substituted transition metals yields out-of-plane ordered $Mo_2TiC_2T_x$ MXene. Ti_3CNT_x MXene is similar to $Ti_3C_2T_x$ with a random mixture of carbon and nitrogen atoms in the X layer. (c) Peak assignments of $Ti_3C_2T_x$, $Mo_2TiC_2T_x$, and Ti_3CNT_x compared to the theoretical peak predictions of $Ti_3C_2O_2$.[13]

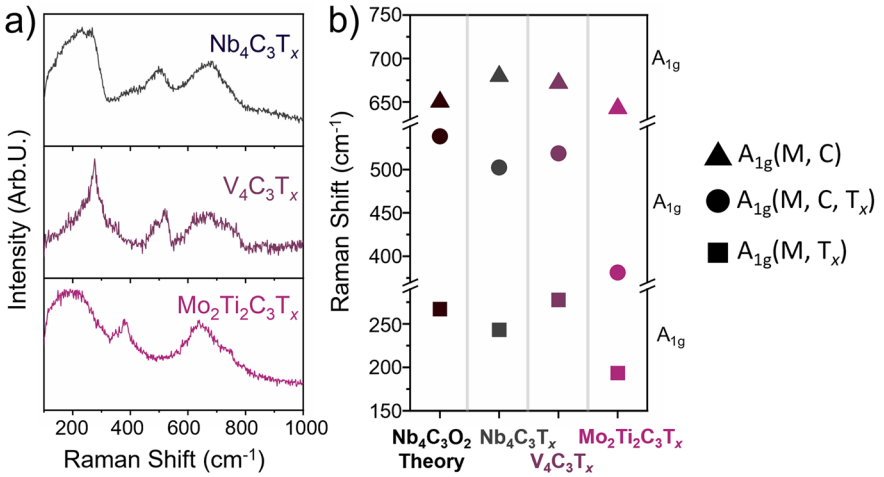

Figure 5. $M_4X_3T_x$ family of MXenes. (a) Raman spectra of $Nb_4C_3T_x$, $V_4C_3T_x$, and $Mo_2Ti_2C_3T_x$ collected with a 514 nm laser. (b) Proposed peak assignments compared to the experimental predictions for $Nb_4C_3O_2$ MXene.[20] The positions of in-plane E_{1g} vibrations are difficult to assign due to the broadening of the peaks.

metal (Ti < Nb < V < Mo) and the bond stiffness of a metal−carbon bond (V = Ti < Nb < Mo) can be seen in Figure 2b. Density functional theory calculations predicted the change of the A_{1g} (M, T_x) peak position with periodic trends, corresponding to the change in the transition metal atomic mass.[16] The A_{1g} peak predictions are taken from the previous literature for Ti_2CO_2, Mo_2CO_2,[16] V_2CFO[15] (V_2CO_2 data was not available) and Nb_2CO_2.[20] Since the terminations are different for V-based MXene calculations, it is an outlier in the M mass-A_{1g} peak position data trend. In our experiments, the peak position gradually shifts from 282 to 248 cm^{-1} with the increase of the mass of M. Similar trend can be observed for the bond stiffness of the M−C bond, where the A_{1g} peak red-shifts with the increasing values of the force constants reported by Wyatt et al.[30] Electronegativity values do not follow the same direct trend, showing that a variety of factors affect peak positions. The deviations from the theoretical calculations are likely due to the inhomogeneous terminations and stacking of multiple monolayer sheets in MXenes, as well as the defects. The intensity of low-frequency E_g and other vibrations in the system is lower than the symmetric A_{1g} vibration and is complicated to assign due to the low SNR, therefore we are not showing E_g peak shift, but it should also follow the same trend of vibration softening with the increase of mass of M.[16] Additionally, it has been previously reported that with the increase in n (e.g., from Ti_2CT_x to $Ti_3C_2T_x$), the vibrational modes experience red shift.[17]

The spectra of the $M_3X_2T_x$ structures ($Ti_3C_2T_x$, $Mo_2TiC_2T_x$, Ti_3CNT_x) are presented in Figure 4a. $Mo_2TiC_2T_x$ has an analogous structure to $Ti_3C_2T_x$ with the outer layers of transition metal substituted by Mo. Therefore, it contains alternating Mo and Ti motifs aligned along the crystallographic c-axis (Figure 4b). The spectra of $Ti_3C_2T_x$ and $Mo_2TiC_2T_x$ similarly resemble three distinct regions: lower frequency vibrations which are assigned to the whole flake (M, X, and T_x) vibrating, vibrations in the 250−500 cm^{-1} range representing surface terminations, and higher frequency vibrations of carbon and surface terminations (C, T_x).[13] The lower frequency region, as shown earlier in the M_2XT_x structures, shifts accordingly to the mass difference: Mo atoms soften the vibration. Thus, the A_{1g} (M, C, and T_x) peak shifts from 203 cm^{-1} in $Ti_3C_2T_x$ to 98 cm^{-1} in $Mo_2TiC_2T_x$. On the contrary, both T_x and C vibrations stiffen when Mo atoms are introduced: A_{1g} (C, T_x) shifts from 721 cm^{-1} in $Ti_3C_2T_x$ to 771 cm^{-1} in $Mo_2TiC_2T_x$. This is due to the fact that Mo−C (2.02 Å) bonds are shorter than Ti−C bonds (2.26 Å).[19] The summary of the peak positions, as well as predicted $Ti_3C_2O_2$ Raman modes,[13] are shown in Figure 4c.

https://doi.org/10.1021/acs.chemmater.3c01742
Chem. Mater. 2023, 35, 8239−8247

Ti_3CNT_x carbonitride MXene is derived from the Ti_3AlCN MAX phase, where the carbon is partially substituted with nitrogen. The distribution of the atoms is random, yielding a disordered structure that affects Raman scattering, lowering the SNR and broadening the peaks observed in $Ti_3C_2T_x$. The peak broadening has also been previously described for sp^2 nanocarbons when their symmetry breaks down from the introduction of defects.[31] Figure 4a shows the Raman spectrum of $Ti_3C_2T_x$ and Ti_3CNT_x where all the sharp features of $Ti_3C_2T_x$ disappear. A similar correlation between the increase of full width at half-maximum (FWHM) of the Raman peaks and disorder in the crystal structure was described for Mo_2S[32] and other nanomaterials.[33] To elucidate the type of defects in Ti_3CNT_x and their effect on Raman spectra, further computational analysis is needed.

Additionally, Raman spectra of $M_4X_3T_x$ MXenes have not been studied as extensively as those of M_2XT_x and $M_3X_2T_x$ structures due to their relative novelty and longer synthesis procedures. The only computational work available shows predicted Raman vibrations for $Nb_4C_3T_x$ pristine and terminated structures.[20] The spectra of $Nb_4C_3T_x$, $V_4C_3T_x$, and $Mo_2Ti_2C_3T_x$ are shown in Figure 5a. They exhibit three broad peaks, which are likely combinations of in-plane and out-of-plane modes. In parallel with the other MXene structures and according to the closest position match to the predicted spectra, we assigned the highest peaks to A_{1g} modes (Figure 5b). The low-frequency A_{1g} mode represents the vibration of the whole flake, the out-of-plane mode in the 400−550 cm^{-1} region is a vibration of outer metal and carbon atoms, as well as the surface terminations, and the high-frequency A_{1g} peak is likely a vibration of metal and carbon atoms.[20] To confirm these assignments, more extensive vibrational predictions are needed.

Lastly, it is important to address the high-frequency region of MXene Raman spectra, where D and G bands of free carbon might be present. The origin of free carbon in MXene samples occurs when they are overetched, resulting from harsh synthesis conditions (high concentration of hydrofluoric acid, high etching temperature, and/or time), insufficient washing steps, or sample contamination. Additionally, amorphous carbon peaks can appear upon photodecomposition of the sample, when high laser power is used.[11] Some of the previous reports on MXene spectra showed D and G bands with much higher intensity than the fingerprint region; in those cases, the MXene synthesis or laser power needs to be adjusted to ensure a better quality of the sample. Figure 6 shows the full spectra (up to 3200 cm^{-1}) of ten MXenes analyzed in this study, as well as the amorphous carbon region. The spectra of V_2CT_x, Nb_2CT_x and Ti_3CNT_x have the highest free carbon peaks due to their higher susceptibility to laser-induced heat damage, however, even in those MXenes broad D and G bands have a much lower intensity than the peaks in the 100−1000 cm^{-1} region. Good quality Raman spectra (lack of oxide peaks and intense amorphous carbon peaks) are important when claiming successful MXene synthesis for various applications.

One of the popular applications of Raman spectroscopy is spectroelectrochemistry, where the structural and chemical changes in MXene electrodes can be uncovered by collecting the spectra *in situ* under the applied potential.[34,35] To illustrate the capabilities of Raman spectroscopy for determining MXene composition, we investigated how the ratio of oxygen and hydroxyl groups affects Raman scattering (Figure 7). A good model system with controlled O/OH ratio of $Ti_3C_2T_x$ is an

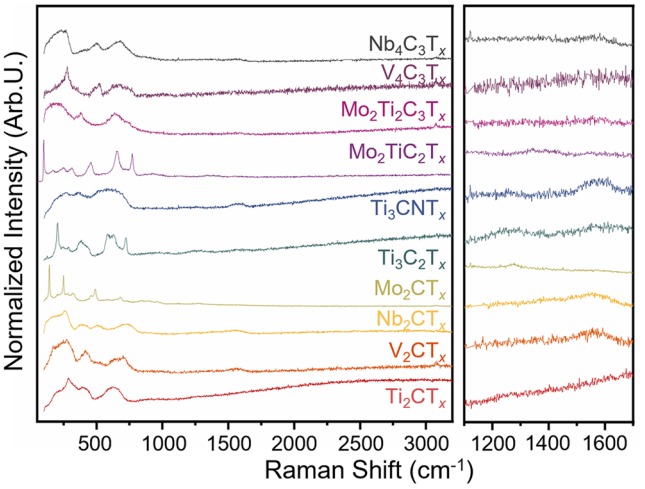

Figure 6. Extended Raman spectra of MXenes from 100−3200 cm^{-1} collected using a 514 nm laser. Carbon region 1200−1700 cm^{-1} shows no or low-intensity D and G bands. With the proper processing steps, it is possible to synthesize MXenes with little to no free carbon.

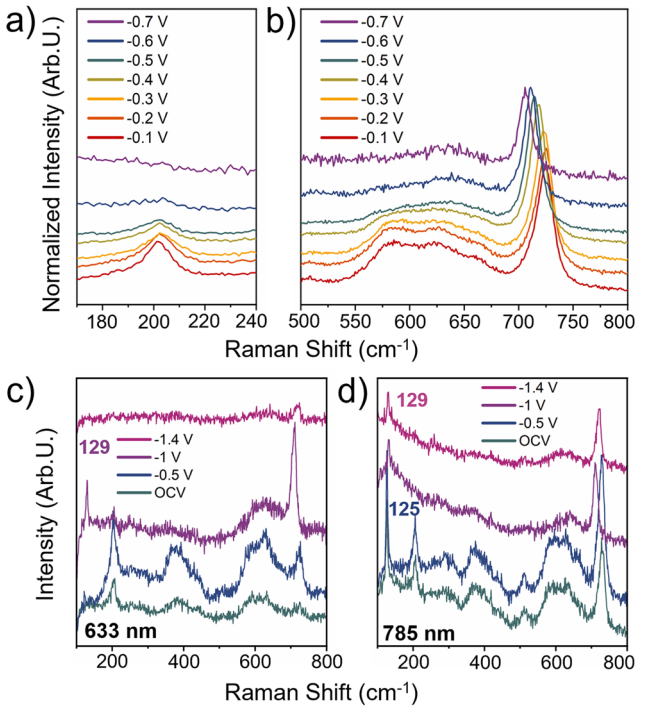

Figure 7. *In-situ* electrochemical study of $Ti_3C_2T_x$ free-standing film with a H_2SO_4/PVA gel electrolyte in a three-electrode configuration. (a) Raman spectra from the A_{1g} (Ti, C, T_x) vibration region collected *in situ* during electrochemical reaction from −0.1 to −0.7 V shows diminishing peak at 200 cm^{-1}. (b) Raman spectra of A_{1g} (C) vibration of $Ti_3C_2T_x$ collected *in situ* during electrochemical from −0.1 V to −0.7 V shows a redshift of the 720 cm^{-1} peak. (c, d) Shift of the resonant Raman laser wavelength during electrochemical cycling. Raman spectra of the $Ti_3C_2T_x$ film under different potentials were collected using (c) 633 and (d) 785 nm laser.

electrochemical reaction of protonation and deprotonation in an acidic electrolyte.[36] The electrochemical cell based on the previous design[34,37] was used (Figure S3). When the cathodic potential is applied to the MXene electrode, the oxygen

https://doi.org/10.1021/acs.chemmater.3c01742
Chem. Mater. 2023, 35, 8239−8247

terminations present on the surface react with the electrolyte, and as a result, the surface of MXene is protonated.

A cathodic potential was applied to the $Ti_3C_2T_x$ electrode in the stable potential window (−0.1 to −0.7 V for H_2SO_4/PVA electrolyte with an Ag wire as a reference electrode) in the 0.1 V steps. The A_{1g} (Ti, C, T_x) vibration slowly diminishes and disappears under the increasing background, while the A_{1g} (C) vibration redshifts with the electrochemical reduction of the MXene surface[38] (Figure 7a,b). That could be explained by the softening of the Ti−O bond which affects the A_{1g} (C) vibration rather than A_{1g} (Ti, C, T_x). Since the surface groups actively participate in an electrochemical reaction and a double-layer is formed at the surface (or between MXene sheets), the symmetry of the MXene−electrolyte complex changes, diminishing A_{1g} (Ti, C, T_x). The higher frequency (>1000 cm^{-1}) peaks are shown in Figure S4.

The resonant Raman peak also shifts when the MXene surface is being protonated during electrochemical cycling in an acidic electrolyte. During this process, the oxygen groups in $Ti_3C_2T_x$ transform to hydroxyl groups and the oxidation state of Ti changes.[36] Simultaneously, the resonant Raman peak position blueshifts to 129 cm^{-1} with the decrease in the potential from open-circuit voltage (OCV) to −1.4 V vs the Ag wire reference electrode (Figure 7d). Another optical feature observed at the same conditions in MXene is the electrochromic effect,[34,37] where MXene plasmon resonance blueshifts with the cathodic potential. Not surprisingly, the excitation wavelength for the resonant Raman effect in $Ti_3C_2T_x$ shifts accordingly (Figure 7c,d).

The choice of laser has been shown to vary the spectra of MXenes based on the resonance effect and penetration depth.[11,27] Since the laser choice can affect the spectra, the spectra collected with 633 and 785 nm lasers (the only two other wavelengths available in our instrument) for analyzed MXenes are reported in Figure S5. The peak intensities and the background change for all of the MXenes, making certain peaks seem to appear/disappear; however, the Raman shift of the peaks remains independent of excitation wavelength. By showing the spectra of ten MXene chemistries with M_2XT_x, $M_3X_2T_x$, and $M_4X_3T_x$ structures collected with three laser wavelengths, we hope this work will serve as a useful reference for fingerprinting MXenes and find its place in the Raman characterization toolbox of MXene researchers.

CONCLUSIONS

In this work, we reported Raman spectra from ten representative MXenes: Ti_2CT_x, Nb_2CT_x, Mo_2CT_x, V_2CT_x, $Ti_3C_2T_x$, $Mo_2TiC_2T_x$, Ti_3CNT_x, $Nb_4C_3T_x$, $V_4C_3T_x$, and $Mo_2Ti_2C_3T_x$, and provided a discussion of band assignment for Raman vibrations. We compared the spectra of the M_2XT_x, $M_3X_2T_x$, and $M_4X_3T_x$ families of MXenes and discussed how transition metals and carbon content affect the spectra in the subset of the analyzed MXenes. In M_2XT_x structures, a symmetric A_{1g} (M, T_x) vibration changes with an increase in the mass of the M-elements. In $M_3X_2T_x$ MXenes, the introduction of defects from doping of the C-layer with N significantly broadens Raman peaks. Additionally, we demonstrated the use of polarized Raman analysis for detecting out-of-plane vibrations in MXenes. This approach can assist in peak assignment. Finally, we showed the use of the Raman technique for spectroelectrochemistry on the example of $Ti_3C_2T_x$ in a protic electrolyte. This systematic study provides a reference for MXene characterization by Raman spectroscopy.

MATERIALS AND METHODS

The materials used in this study were synthesized by selective etching of A-element layers from the parent MAX phases, followed by the delamination step. All synthesis conditions are summarized in Table S1. After synthesis, MXenes were processed into free-standing films by vacuum-assisted filtration. Those films were used for Raman spectroscopy and XRD measurements.

Raman Spectrometer. We used an inverted reflection mode Renishaw InVia (Gloucestershire, U.K.) instrument with a 63× (NA = 0.7) objective and a Peltier-cooled CCD camera. For the main measurements, we used a 514 nm laser with a 1800 line/mm diffraction grating, with a 120 s acquisition time and 1.47 mW laser power. For the He−Ne (633 nm) and diode (785 nm) lasers, we used the 1800 line/mm grating with 4.06 mW laser power and the 1200 line/mm grating with 3.59 mW laser power, respectively. Some spectra (specified on the *y*-axis) were normalized by division by the maximum intensity.

XRD. X-ray diffraction (XRD) patterns were acquired with Ni-filtered Cu Kα radiation (λ = 1.54 Å; Miniflex, Rigaku, Japan) operated at 40 kV and 15 mA with a step scan of 0.03° (scanned from 3 to 70°) and holding time of 0.5 s.

ASSOCIATED CONTENT

Supporting Information

The Supporting Information is available free of charge at https://pubs.acs.org/doi/10.1021/acs.chemmater.3c01742.

The following files are available free of charge: synthesis conditions for ten MXenes, polarized Raman schematic, spectra of Mo_2CT_x MXene collected with different lasers, description of the 3-electrode electrochemical cell, carbon region spectra during *in situ* study, and spectra of ten MXenes collected with 633 and 785 nm lasers (PDF)

AUTHOR INFORMATION

Corresponding Author

Yury Gogotsi − *A. J. Drexel Nanomaterials Institute and Department of Materials Science and Engineering, Drexel University, Philadelphia, Pennsylvania 19104, United States;* orcid.org/0000-0001-9423-4032; Email: gogotsi@drexel.edu

Authors

Kateryna Shevchuk − *A. J. Drexel Nanomaterials Institute and Department of Materials Science and Engineering, Drexel University, Philadelphia, Pennsylvania 19104, United States;* orcid.org/0000-0001-7411-3110

Asia Sarycheva − *A. J. Drexel Nanomaterials Institute and Department of Materials Science and Engineering, Drexel University, Philadelphia, Pennsylvania 19104, United States; Energy Storage and Distributed Resources Division, Lawrence Berkeley National Laboratory, Berkeley, California 94720, United States;* orcid.org/0000-0002-5151-8980

Christopher E. Shuck − *A. J. Drexel Nanomaterials Institute and Department of Materials Science and Engineering, Drexel University, Philadelphia, Pennsylvania 19104, United States;* orcid.org/0000-0002-1274-8484

Complete contact information is available at: https://pubs.acs.org/10.1021/acs.chemmater.3c01742

https://doi.org/10.1021/acs.chemmater.3c01742
Chem. Mater. 2023, 35, 8239−8247

Author Contributions

[#]K.S. and A.S. contributed equally. The manuscript was written through contributions of all authors. All authors have given approval to the final version of the manuscript.

Notes

The authors declare no competing financial interest.

■ ACKNOWLEDGMENTS

The authors are thankful to Danzhen Zhang, Kyle Matthews, and Teng Zhang for assisting with material synthesis and Alex Inman for assisting with figure design. This work was supported by a U.S. National Science Foundation grant DMR-2041050. XRD was performed using instruments in the Materials Characterization Core at Drexel University.

■ REFERENCES

(1) Ferrari, A. C.; Basko, D. M. Raman Spectroscopy as a Versatile Tool for Studying the Properties of Graphene. *Nat. Nanotechnol.* **2013**, *8*, 235−246.
(2) Ferrari, A. C.; Robertson, J. Interpretation of Raman Spectra of Disordered and Amorphous Carbon. *Phys. Rev. B: Condens. Matter* **2000**, *61*, 14095−14107.
(3) Balandin, A. A.; Ghosh, S.; Bao, W.; Calizo, I.; Teweldebrhan, D.; Miao, F.; Lau, C. N. Superior Thermal Conductivity of Single-Layer Graphene. *Nano Lett.* **2008**, *8*, 902−907.
(4) Malard, L. M.; Pimenta, M. A.; Dresselhaus, G.; Dresselhaus, M. S. Raman Spectroscopy in Graphene. *Phys. Rep.* **2009**, *473*, 51−87.
(5) Del Corro, E.; Terrones, H.; Elias, A.; Fantini, C.; Feng, S.; Nguyen, M. A.; Mallouk, T. E.; Terrones, M.; Pimenta, M. A. Excited Excitonic States in 1L, 2L, 3L, and Bulk WSe_2 Observed by Resonant Raman Spectroscopy. *ACS Nano* **2014**, *8*, 9629−9635.
(6) VahidMohammadi, A.; Rosen, J.; Gogotsi, Y. The World of Two-Dimensional Carbides and Nitrides (MXenes). *Science* **2021**, *372*, eabf1581.
(7) Mathis, T.; Maleski, K.; Goad, A.; Sarycheva, A.; Anayee, M.; Foucher, A.; Hantanasirisakul, K.; Stach, E.; Gogotsi, Y.; Shuck, C. E. Modified MAX Phase Synthesis for Environmentally Stable and Highly Conductive Ti_3C_2 MXene. *ACS Nano* **2021**, *15*, 6420−6429.
(8) Naguib, M.; Barsoum, M. W.; Gogotsi, Y. Ten Years of Progress in the Synthesis and Development of MXenes. *Adv. Mater.* **2021**, *33*, 2103393.
(9) Shekhirev, M.; Shuck, C. E.; Sarycheva, A.; Gogotsi, Y. Characterization of MXenes at Every Step, from Their Precursors to Single Flakes and Assembled Films. *Prog. Mater. Sci.* **2021**, *120*, 100757.
(10) Wang, C.; Chen, S.; Song, L. Tuning 2D MXenes by Surface Controlling and Interlayer Engineering: Methods, Properties, and Synchrotron Radiation Characterizations. *Adv. Funct. Mater.* **2020**, *30*, 2000869.
(11) Sarycheva, A.; Gogotsi, Y. Raman Spectroscopy Analysis of the Structure and Surface Chemistry of $Ti_3C_2T_x$ MXene. *Chem. Mater.* **2020**, *32*, 3480−3488.
(12) Sarycheva, A.; Shanmugasundaram, M.; Krayev, A.; Gogotsi, Y. Tip-Enhanced Raman Scattering Imaging of Single- to Few-Layer $Ti_3C_2T_x$ MXene. *ACS Nano* **2022**, *16*, 6858−6865.
(13) Hu, T.; Wang, J.; Zhang, H.; Li, Z.; Hu, M.; Wang, X. Vibrational Properties of Ti_3C_2 and $Ti_3C_2T_2$ (T = O, F, OH) Monosheets by First-Principles Calculations: a Comparative Study. *Phys. Chem. Chem. Phys.* **2015**, *17*, 9997−10003.
(14) Berger, E.; Lv, Z.-P.; Komsa, H.-P. Raman Spectra of 2D Titanium Carbide MXene from Machine-Learning Force Field Molecular Dynamics. *J. Mater. Chem. C* **2023**, *11*, 1311−1319.
(15) Champagne, A.; Shi, L.; Ouisse, T.; Hackens, B.; Charlier, J.-C. Electronic and Vibrational Properties of V_2C-Based MXenes: From Experiments to First-Principles Modeling. *Phys. Rev. B: Condens. Matter* **2018**, *97*, 115439.
(16) Yorulmaz, U.; Özden, A.; Perkgöz, N. K.; Ay, F.; Sevik, C. Vibrational and Mechanical Properties of Single Layer MXene Structures: a First-Principles Investigation. *Nanotechnol.* **2016**, *27*, 335702.
(17) Hu, T.; Hu, M.; Li, Z.; Zhang, H.; Zhang, C.; Wang, J.; Wang, X. Covalency-Dependent Vibrational Dynamics in Two-Dimensional Titanium Carbides. *J. Phys. Chem. A* **2015**, *119*, 12977−12984.
(18) Huang, H.; Wang, W.; Zhang, S. Theoretical Assessment of Raman Spectra on MXene Ti_2C: from Monolayer to Bilayer. *Phys. Chem. Chem. Phys.* **2021**, *23*, 19884−19891.
(19) Li, L. Lattice Dynamics and Electronic Structures of $Ti_3C_2O_2$ and $Mo_2TiC_2O_2$ (MXenes): The Effect of Mo Substitution. *Comput. Mater. Sci.* **2016**, *124*, 8−14.
(20) Hu, T.; Hu, M.; Gao, B.; Li, W.; Wang, X. Screening Surface Structure of MXenes by High-Throughput Computation and Vibrational Spectroscopic Confirmation. *J. Phys. Chem. C* **2018**, *122*, 18501−18509.
(21) Liu, L.; Orbay, M.; Luo, S.; Duluard, S.; Shao, H.; Harmel, J.; Rozier, P.; Taberna, P.-L.; Simon, P. Exfoliation and Delamination of $Ti_3C_2T_x$ MXene Prepared via Molten Salt Etching Route. *ACS Nano* **2022**, *16*, 111−118.
(22) Wang, D.; Zhou, C.; Filatov, A. S.; Cho, W.; Lagunas, F.; Wang, M.; Vaikuntanathan, S.; Liu, C.; Klie, R. F.; Talapin, D. V. Direct Synthesis and Chemical Vapor Deposition of 2D Carbide and Nitride MXenes. *Science* **2023**, *379*, 1242−1247.
(23) Alhabeb, M.; Maleski, K.; Anasori, B.; Lelyukh, P.; Clark, L.; Sin, S.; Gogotsi, Y. Guidelines for Synthesis and Processing of Two-Dimensional Titanium Carbide ($Ti_3C_2T_x$ MXene). *Chem. Mater.* **2017**, *29*, 7633−7644.
(24) Lim, K. R. G.; Shekhirev, M.; Wyatt, B. C.; Anasori, B.; Gogotsi, Y.; Seh, Z. W. Fundamentals of MXene Synthesis. *Nat. Synth.* **2022**, *1*, 601−614.
(25) Maleski, K.; Shuck, C. E.; Fafarman, A. T.; Gogotsi, Y. The Broad Chromatic Range of Two-Dimensional Transition Metal Carbides. *Adv. Opt. Mater.* **2021**, *9*, 2001563.
(26) Tuschel, D. Raman Crystallography, in Theory and in Practice. *Spectroscopy* **2012**, *27*, 22.
(27) Yoo, R. M. S.; Djire, A. Decoupling the Surface and Bulk Reactivities of MXenes and Catalytic Activity Tuning through Surface Chemistry Modification. *ACS Catal.* **2023**, *13*, 6823−6836.
(28) Lee, J.-U.; Park, J.; Son, Y.-W.; Cheong, H. Anomalous Excitonic Resonance Raman Effects in Few-Layered MoS_2. *Nanoscale* **2015**, *7*, 3229−3236.
(29) Velusamy, D. B.; El-Demellawi, J. K.; El-Zohry, A. M.; Giugni, A.; Lopatin, S.; Hedhili, M. N.; Mansour, A. E.; Fabrizio, E. D.; Mohammed, O. F.; Alshareef, H. N. MXenes for Plasmonic Photodetection. *Adv. Mater.* **2019**, *31*, 1807658.
(30) Wyatt, B. C.; Rosenkranz, A.; Anasori, B. 2D MXenes: Tunable Mechanical and Tribological Properties. *Adv. Mater.* **2021**, *33*, 2007973.
(31) Jorio, A.; Saito, R.; Dresselhaus, G.; Dresselhaus, M. S. Disorder Effects in the Raman Spectra of sp^2 Carbons. In *Raman Spectroscopy in Graphene Related Systems*; Wiley: 2011; pp 299−325.
(32) Mignuzzi, S.; Pollard, A. J.; Bonini, N.; Brennan, B.; Gilmore, I. S.; Pimenta, M. A.; Richards, D.; Roy, D. Effect of Disorder on Raman Scattering of Single-Layer MoS_2. *Phys. Rev. B: Condens. Matter* **2015**, *91*, 195411.
(33) Gouadec, G.; Colomban, P. Raman Spectroscopy of Nanomaterials: How Spectra Relate to Disorder, Particle Size and Mechanical Properties. *Prog. Cryst. Growth Charact. Mater.* **2007**, *53*, 1−56.
(34) Salles, P.; Pinto, D.; Hantanasirisakul, K.; Maleski, K.; Shuck, C. E.; Gogotsi, Y. Electrochromic Effect in Titanium Carbide MXene Thin Films Produced by Dip-Coating. *Adv. Funct. Mater.* **2019**, *29*, 1809223.
(35) Johnson, D.; Lai, H.-E.; Hansen, K.; Balbuena, P. B.; Djire, A. Hydrogen Evolution Reaction Mechanism on Ti_3C_2 MXene Revealed by In Situ/Operando Raman Spectroelectrochemistry. *Nanoscale* **2022**, *14*, 5068−5078.

https://doi.org/10.1021/acs.chemmater.3c01742
Chem. Mater. 2023, 35, 8239−8247

(36) Zhan, C.; Naguib, M.; Lukatskaya, M.; Kent, P. R. C.; Gogotsi, Y.; Jiang, D. E. Understanding the MXene Pseudocapacitance. *J. Phys. Chem. Lett.* **2018**, *9*, 1223−1228.
(37) Valurouthu, G.; Maleski, K.; Kurra, N.; Han, M.; Hantanasirisakul, K.; Sarycheva, A.; Gogotsi, Y. Tunable Electrochromic Behavior of Titanium-Based MXenes. *Nanoscale* **2020**, *12*, 14204−14212.
(38) Lukatskaya, M. R.; Bak, S.-M.; Yu, X.; Yang, X.-Q.; Barsoum, M. W.; Gogotsi, Y. Probing the Mechanism of High Capacitance in 2D Titanium Carbide Using In Situ X-Ray Absorption Spectroscopy. *Adv. Energy Mater.* **2015**, *5*, 1500589.

https://doi.org/10.1021/acs.chemmater.3c01742
Chem. Mater. 2023, 35, 8239−8247